J Inno Sci Eng,2022, 6(2):175-189
https://doi.org/10.38088/jise.1102935

Research Article

The Structural Characterization, Radioluminescence Results, and Thermoluminescence Kinetic Parameters of Aventurine

Ilker Cetin KESKIN[1*]

[1*] *Department of Electricity and Energy, Soma Vocational School, Manisa Celal Bayar University, Soma 45500, Manisa, Turkey.*

Cite this paper as:
Keskin, Ç. I. (2022). *The Structural Characterization, Radioluminescence Results, and Thermoluminescence Kinetic Parameters of Aventurine*. Journal of Innovative Science and Engineering.6(2):175-189

*Corresponding author: Ilker Cetin Keskin
E-mail: ilker.keskin@cbu.edu.tr

Received Date:13/04/2021
Accepted Date:03/06/2022

Abstract

In this study, in which the optical and luminescence properties of aventurine, a silicate-based mineral, were examined, the crystal structure of the mineral was examined by XRD analysis, its rheological properties and the elements it contained were determined by SEM-EDX analysis, and its structural properties were examined by FT-IR analysis. In order to determine the luminescence properties, radioluminescence (RL) and thermoluminescence (TL) methods were used and kinetic parameters were calculated. In the measurements taken in bulk and powder form of Aventurine, it was observed that the powder sample had a much better spectrum intensity, it was observed that the emission around 570 nm became much more pronounced in the powder sample. On the other hand, similar emissions were detected in both samples, though at different intensities. In TL analysis, it was observed that Aventurine was responsive to both X-ray and ultraviolet radiation at three different doses. While after X-ray irradiation, Aventurine exhibited TL glow curves with peaks at maximum temperatures of 90 oC and 250 oC, under UV irradiation the TL glow curves concentrated in the high-temperature region which is around 300 oC observed. Also; the TL kinetic parameters were reported; activation energy (E), the order of kinetics (b), and frequency factor (s) of the first peak have been determined in detail by using Computerized Glow Curve Deconvolution (CGCD) method.

Keywords: Quartz, Structural Characterization, Thermal Analysis Radioluminescence (RL), Thermoluminescence (TL)

1. Introduction

Aventurine is a mineral that has been used for many years as a glazing material. Aventurine, which is a silicon-based (SiO_2) mineral, contains elements such as chromium, iron, magnesium, aluminum, and potassium, but also contains trace amounts of different elements. Aventurine, a type of quartz, is found in nature in green, orange, gray, and blue tones. Aventurine, which is frequently seen in green examples, has a granular structure with metallic lusters. It has a scaly appearance, has a microcrystalline structure, and also contains hematite and mica. Due to its silicate structure, it shows different colors depending on the number of impurity atoms that serve as color centers in the crystal structure. When we look at the studies on aventurine, it is seen that there are some characterization studies in general terms, but there are intense thermal studies on this mineral because it is widely used as a glazing material [1–4].

In a study on Beryl, one of the silicate group minerals, it was reported that it has a wide emission range between 300 and 800 nm, with maximum peaks around 470 nm and 580 nm in the cathodoluminescence (CL) spectrum. It has been stated that the Cr^{3+} ion plays an important role in the color centers of the green-colored beryl mineral [5]. In the study on chalcedony, one of the most well-known minerals of the quartz family, a maximum TL peak was recorded at 110 °C for white chalcedony and 121 °C for blue chalcedony in the TL studies taken after X-ray excitation [6]. In TL measurements taken after irradiation of onyx mineral, which is also a variation of chalcedony, with gamma radiation, peaks were detected at 150 and 210 °C [7].

Since aventurine is a feldspar group and a mineral found in different colors in nature and used as a glaze material by heat treatment, the effect of the presence of color centers on the optical properties (radioluminescence) of the mineral is interesting for research. On the other hand, the investigation of thermoluminescence properties, which occur as a result of the thermal effect of interaction with radiation, gives a different perspective to the optical properties of aventurine minerals.

In this study, unlike the literature, the optical and luminescence properties of aventurine are emphasized. In terms of luminescence, it has been observed that it has a strong thermoluminescence response due to radiation excitation. In addition, some characterization analyzes are also included. Radioluminescence and thermoluminescence properties of aventurine samples excited by X-ray and short-wavelength ultraviolet radiation were examined and kinetic parameter calculations were made on the glow curve. As stated above, no dosimetric and optical characterization studies of aventurine have been found in the literature. The sample used in the study was obtained commercially and is known to have been mined from the Mysore region of India.

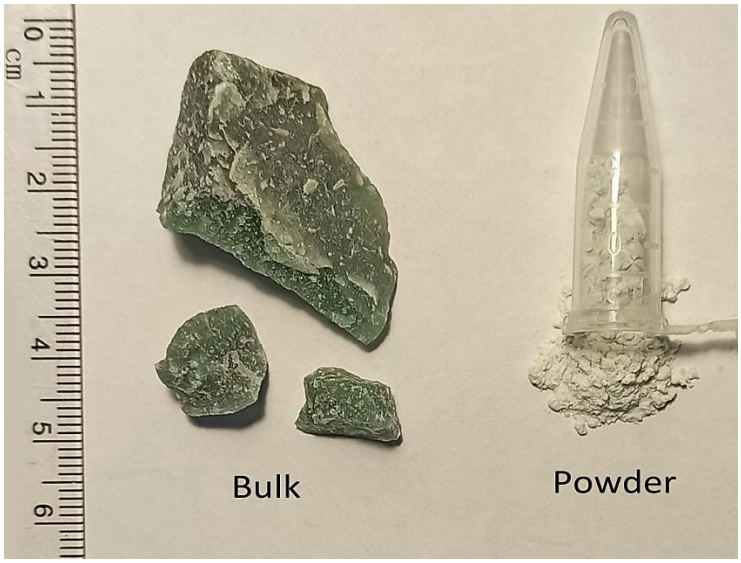

Figure 1. Bulk and powder form Aventurine.

Figure 1 shows the bulk and powder forms of aventurine minerals. In the press used for pellet preparation, the mechanically crushed mineral was powdered and sieved with a pore size of 150 microns. A powder sample was used in all analyzes. In order to compare the RL emissions of both, the bulk sample was also analyzed in the RL measurement only. In our previous studies on minerals, it was observed that better luminescence results were obtained from powdered samples.

2. Materials and Methods

PANanalytical Empyrean brand X-ray diffraction (XRD) device was used to determine the crystal structure of aventurine and to determine the major or minor phases present. The step scan range was determined as 10^{o}-80^{o} when the XRD pattern was taken from the powdered aventurine sample. Working conditions of diffractometer; current is determined as 40 mA and voltage as 45 kV. The X-ray source of the device has a Cu-Ka anode and has a wavelength of 1.5405 Å.
The FTIR spectra were carried out with a potassium bromide (KBr) disc for absorbance in the region 400–4000 cm^{-1} using a Perkin Elmer Spectrum 100 FTIR spectrophotometer. Gemini SEM500 device was used to examine the surface morphology and to obtain EDX spectrum of the aventurine.
TL glow curves of the aventurine exposed to short-wavelength UV light (254 nm) and X-rays were recorded in the range of 50 ^{o}C to 400 ^{o}C in a dark room with an RA94 Reader / Analyzer system in N2 atmosphere. In order to obtain the TL glow curve of the powder sample, thin aluminum pots prepared in a way that would not create a surface gap with the thermocouple in the sample room of the device were used. The TL responses of aventurine according to different excitation were taken at a heating rate of 2 oC/s after 10, 20, and 30 min irradiation for both sources.
In the radioluminescence (RL) system, the X-rays obtained from the tungsten target by operating the Machlett OEG-50A X-ray tube at 30 kV and 15 mA, which have a dose value of 30 Gy per minute, are directed to the sample. The occurring scintillation is transmitted to the Jobin Yvon spectrophotometer thanks to the optical path positioned at an angle. Signals are collected by a CCD (Charge Coupled Device) detector cooled with liquid nitrogen, and the luminescence spectrum is obtained by this process.

3. Results and Discussion

3.1. XRD Analysis of Aventurine

The X-ray diffraction (XRD) pattern and phase analysis of the aventurine was performed and represented in Figure 2. Quartz is a non-clay mineral commonly and invariably found in all specimens. Aventurine is a silicate-based mineral. The result of phase analysis for aventurine powder X'Pert Highscore Plus program was matched that planes of the hexagonal Silicon Dioxide (SiO^2) such as (010), (011), (111), (112), (121), and (220) with XRD pattern of aventurine. In addition, low-intensity phases of cubic Fe2+ and tetragonal CrO2 referred to with ICSD cards no (96-900-6607) and (01-076-1232) respectively, were detected in the XRD pattern.

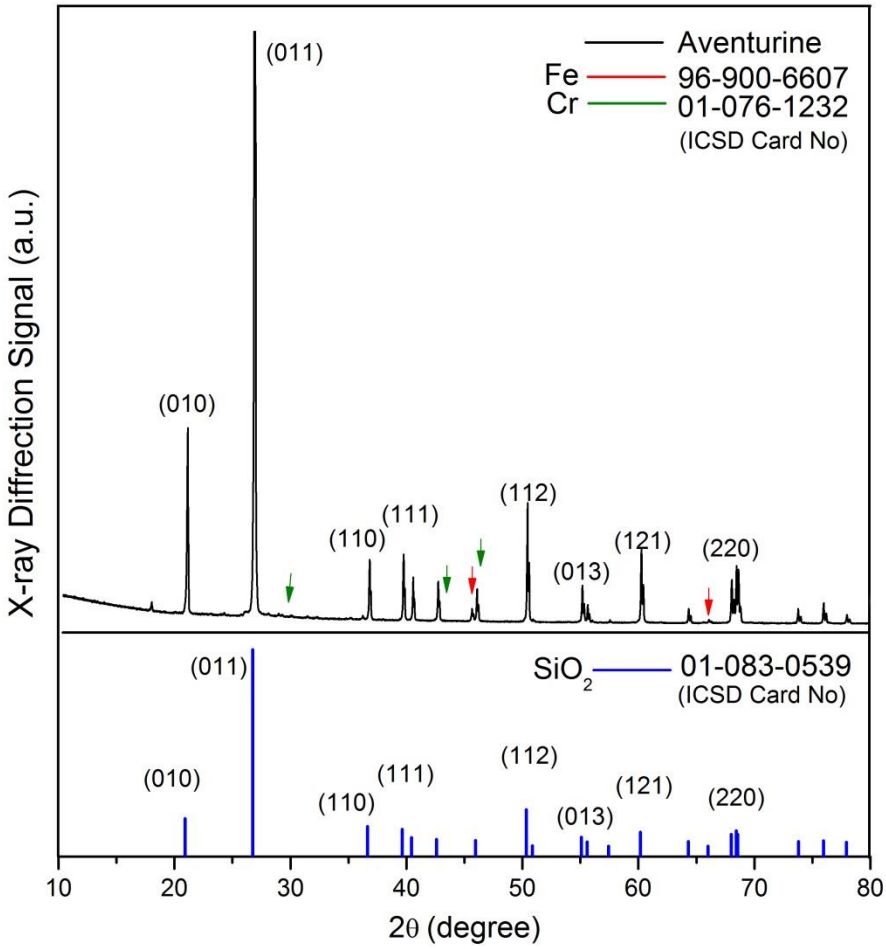

Figure 2. X-ray diffraction (XRD) pattern of aventurine.

The Debye-Scherrer's equation was used to calculate the average crystallite sizes of aventurine powder (1):

$$D = \frac{k\lambda}{\beta Cos\theta} \quad (1)$$

where D is the crystallite size (nm), k= 0.94, λCu = 0.15406 nm, β is the full width at half-maximum of the peak in radians corrected from instrumental broadening, and θ is the peak angle [6,8]. To calculate the average crystallite size,

(011) plane of the XRD pattern was used because of it has strongest intensity. The average crystallite size was found 90.57 nm. The data used for calculation; Peak max (2θ): 26.5517221, θ2: 26.5912564, θ1: 26.4971291, FWHM: 0.0941273, Cos (θ): 0.973276.

3.2. FT-IR Spectrum of Aventurine

Figure 3 shows the FTIR spectrum of aventurine. In accordance with the literature, the marked peaks which are Si-O interactions and the band assignment peaks of Al and Mg in the structure of the quartz-based aventurine mineral were specified. The findings are listed in Table 1.

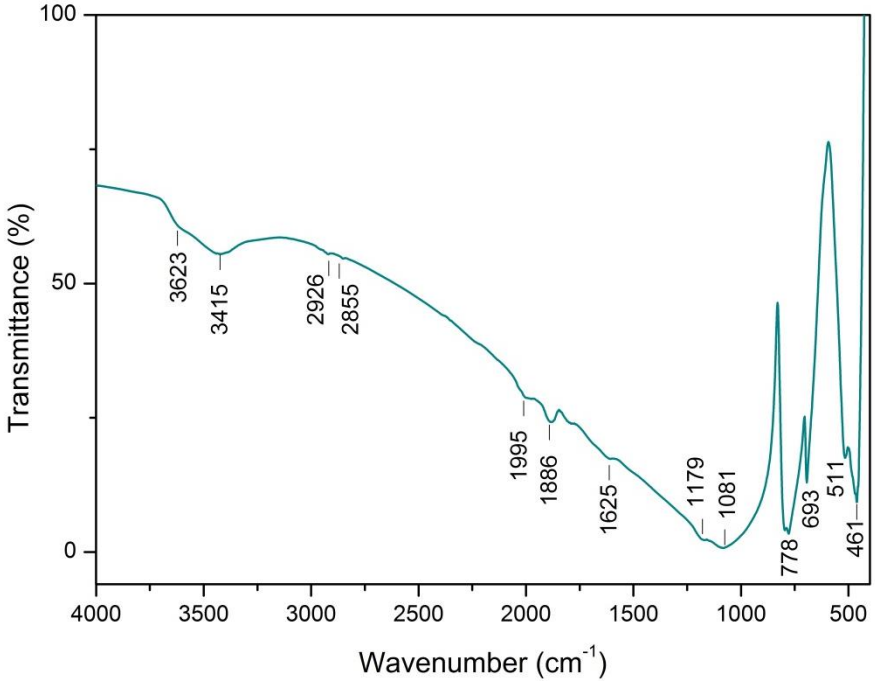

Figure 3. FTIR spectrum of Aventurine

Table 1. FT-IR transmission bands assignments of aventurine [9,10].

Wavenumber (cm^{-1})	**Probable Band Assignment**
461, 511	asymmetrical bending vibrations of Si-O
693	symmetrical bending vibrations of Si-O
778	symmetrical stretching vibrations of Si-O
1081,1179	asymmetrical stretching vibrations of Si-O due to low Al for Si substitution
1625	inbound molecular water to Al or Mg.
1886, 1995	combination of vibrations of the Si-O network
2855, 2926	organic carbon
3415	O--H group
3623	stretching vibration of O–H

3.3. SEM Images and EDX Spectrum of Aventurine

Fig. 4 is shown the morphology and composition of aventurine were assigned under scanning electron microscopy and energy-dispersive X-ray spectroscopy (SEM-EDX). This analysis gave valuable information about atoms that composed the mineral and that allowed the observation of the morphological structure of the aventurine mineral. The SEM images of microstructural features of two different sides (Fig. 4 a-b) were taken at a magnification 5000X, and it's seen that the aventurine has a layered microstructure.

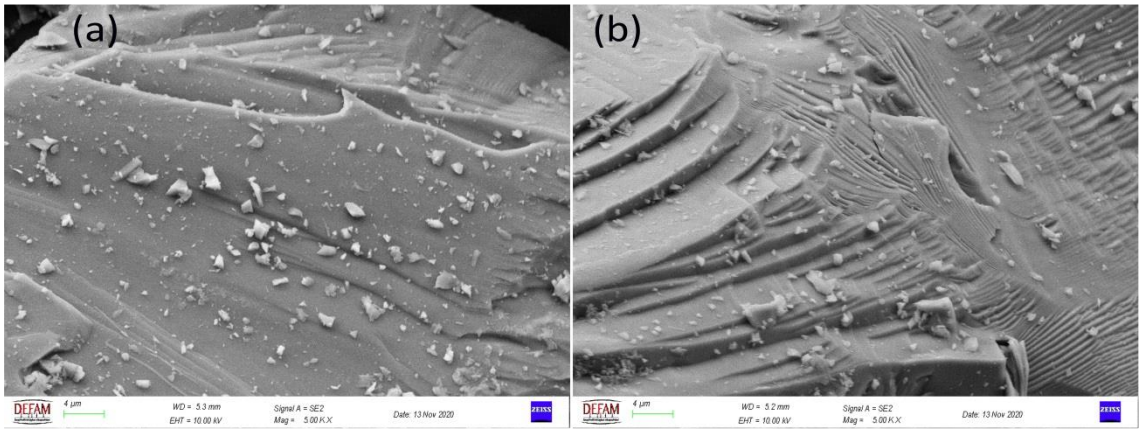

Figure 4. SEM images of Aventurine from different sides same diameter, and magnification.

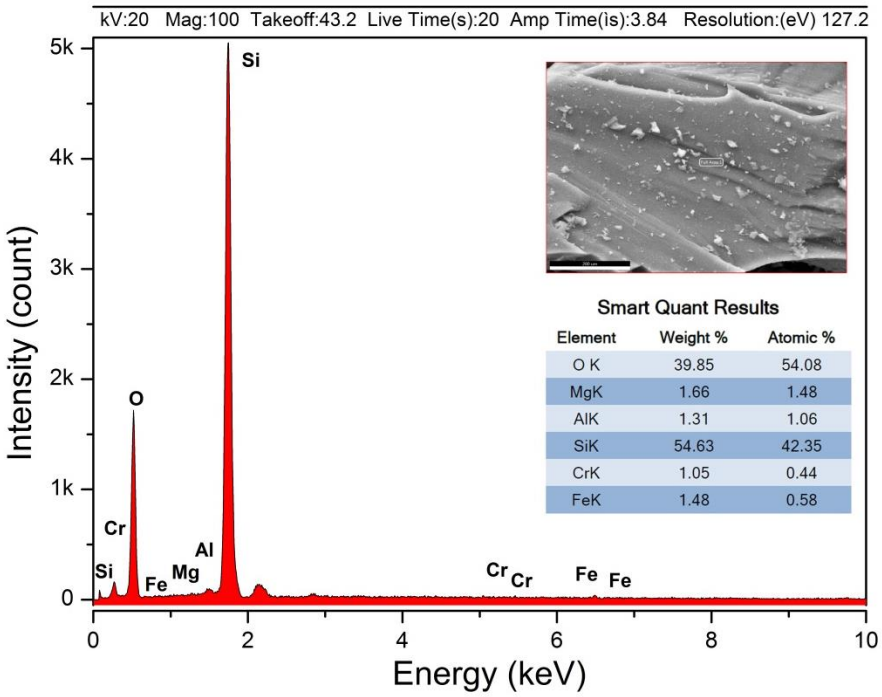

Figure 5. EDX spectrum of Aventurine.

As seen in Fig.5, as expected according to the quantitative results, the presence of a high amount of Si shows itself. Following Si, Mg, Al, Fe, and Cr impurities have been detected. These atoms directly affect the luminescence properties of the mineral.

The coloration in minerals is due to defects in the crystal structure, impurity atoms, or both. The electrons that produce color by the absorption of light can sometimes be found on a foreign atom or in a defective crystal. An impurity or structural defect can create energy levels locally between the valance and conduction bands. If the energy differences between this energy level and the conductivity and valence bands are in visible light, coloration occurs. Thus, light energy stimulated an electron; providing an energy transition and causing the electron to transition to a higher energy level. The formation of coloration occurs by the absorption of some of the wavelengths that make up the light. These impurity atoms act as color centers. Atoms detected in EDX analysis can exist in ionic states with different charges. The emission behaviors of the ionic states of these detected atoms are discussed under the title of RL properties.

3.4. TL Dose Responses and Kinetic Parameters

The thermoluminescence formation mechanism can be briefly defined as the first exposure of the material to radiation and then the obtaining of a glow curve with thermal excitation. According to the band model; Absorption of radiation means the formation of electron-hole pairs. The energy storage property is due to the presence of crystal defects such as impurities or vacancies. These defects are formed during the irradiation process and can trap electrons and holes. The material is excited with a radiation source such as an X-ray, β, γ, or UV light. As a result of the excitation, the electrons are trapped in the traps originating from the impurity atoms in the material. After the excitation process, by thermally stimulating the material the electrons in these traps are released and a glow curve is obtained. The glow curve gives information about the characteristic properties such as activation energy and trap depth.

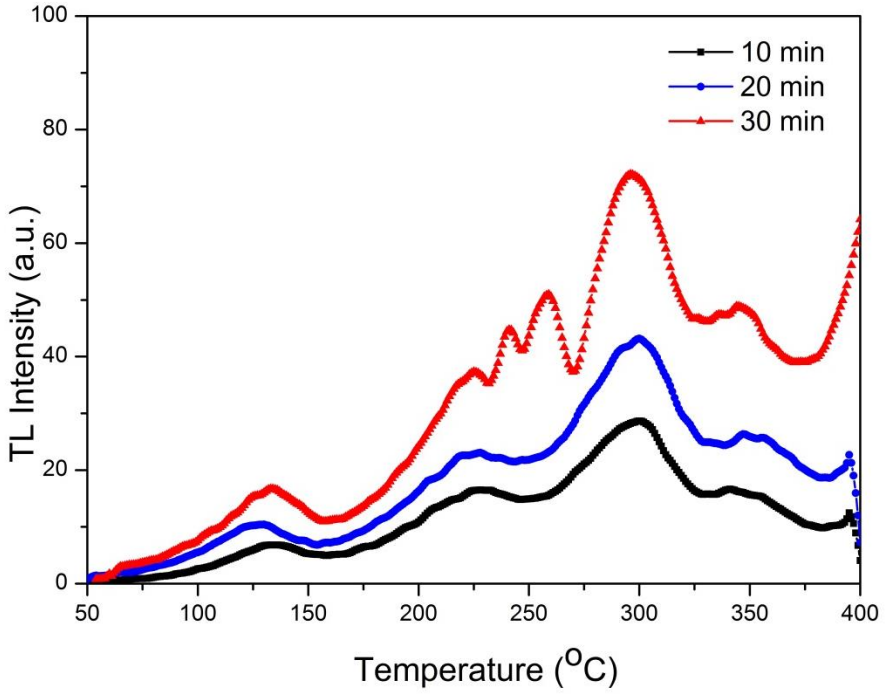

Figure 6. TL curves of Aventurine taken after 254 nm UV irradiation at 10, 20, 30 min.

Figure 6 shows the TL glow curves from 50 °C up to 400 °C of the powder aventurine irradiated with shortwave UV light for 10, 20, and 30 min. The glow curves have been recorded at a heating rate of 2 °C/s following irradiation. In Table 2, the maximum peak points of the glow curves obtained after UV irradiation are given. This peak became more

pronounced with the increasing dose of aventurine, which retained its general glow characteristic of around 350 °C. Also, it has been observed that new trap levels occur at 241 and 258 °C.

Table 2. The maximum TL curves of aventurine irradiated with UV light.

Irradiation Time (min)	Maximum Points of TL Peaks (°C)					
10	135	228	-	-	300	350
20	127	223	-	-	299	353
30	133	224	241	258	295	345

An important detail that draws attention to the glow curve formed as a result of 30 minutes of irradiation; The rise starting from 375 °C is the presence of peaks of possible new trap levels at higher temperatures. However, the current device's inability to measure over 400 °C does not make it possible to observe this peak.

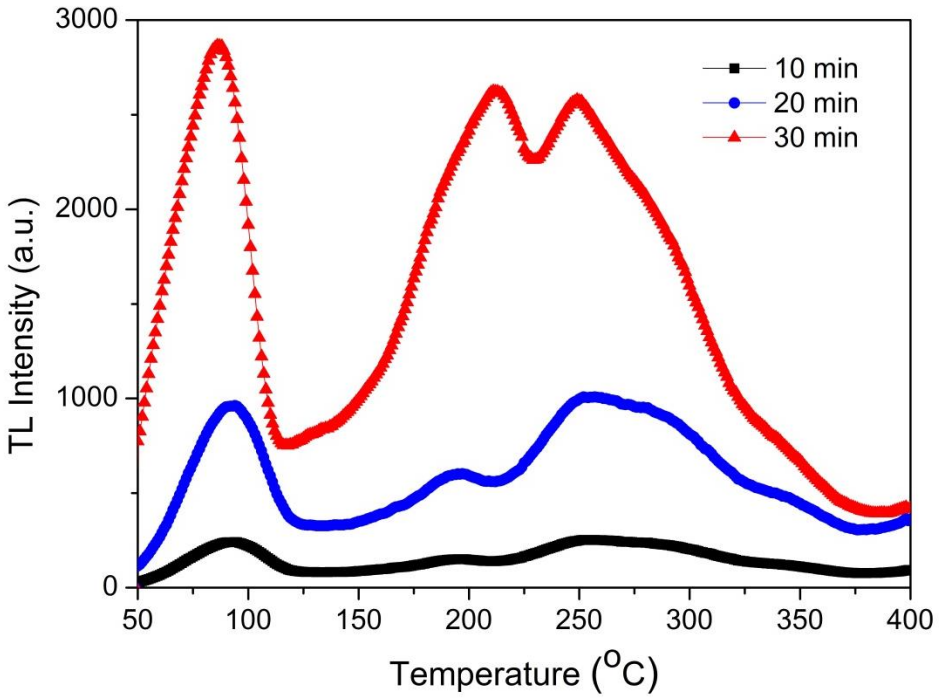

Figure 7. TL curves of Aventurine at different doses under X-ray excitation.

As seen in Figure 7, the TL glow curves from 50 °C up to 400 °C of the powder aventurine irradiated with X-rays for three different doses (300 Gy, 600 Gy, 900 Gy). The glow curves have been recorded at a heating rate of 2 °C/s following irradiation. In Table 3, the maximum peak points of the glow curves obtained after each X-ray irradiation are given.

Table 3. The maximum TL curves of aventurine irradiated with X-ray.

Irradiation Time (min)	Maximum Points of TL Peaks (°C)				
10	94	193	259	-	344
20	91	195	252	-	345
30	86	212	249	289	343

As the irradiation increased, it was observed that the FWHM value of the glow curve of around 90 °C, characteristically encountered in quartz-based minerals, decreased and became more pronounced. The wide peak with a maximum point of around 250 °C and a shoulder around 195 °C, indicating the presence of deep traps, behaved like a single wide peak with the increase in dose. In the glow curve obtained after 900 Gy irradiation, it is noteworthy that a deep trap is evident at 212 °C degrees. Depending on the dose increase, it is expected that new deep traps will become evident or that existing ones will behave as a component of a single glow curve.

The luminescence glow curve of the sample from which TL measurement was taken is the combined state of many different luminescence peaks of the traps arising from the impurity atoms and crystalline dislocations in that mineral. In order to determine the activation energies and intensities of each of the peak components that make up this main radiation curve, the CGDC method is a frequently used method and there are many programs for this application. Of course, when deconvoluting the complex structure of the main glow curve, the correct number of peaks and the correct position of each peak is an important factor in the calculation of TL kinetic parameters. [11–13]. Since TL signal intensity exhibits a significant peak at both high and low temperatures and also has a good dose-response to X-ray radiation for dosimetric studies, the TL glow curve obtained as a result of 900 Gy dosing was deconvoluted. (Fig.8)

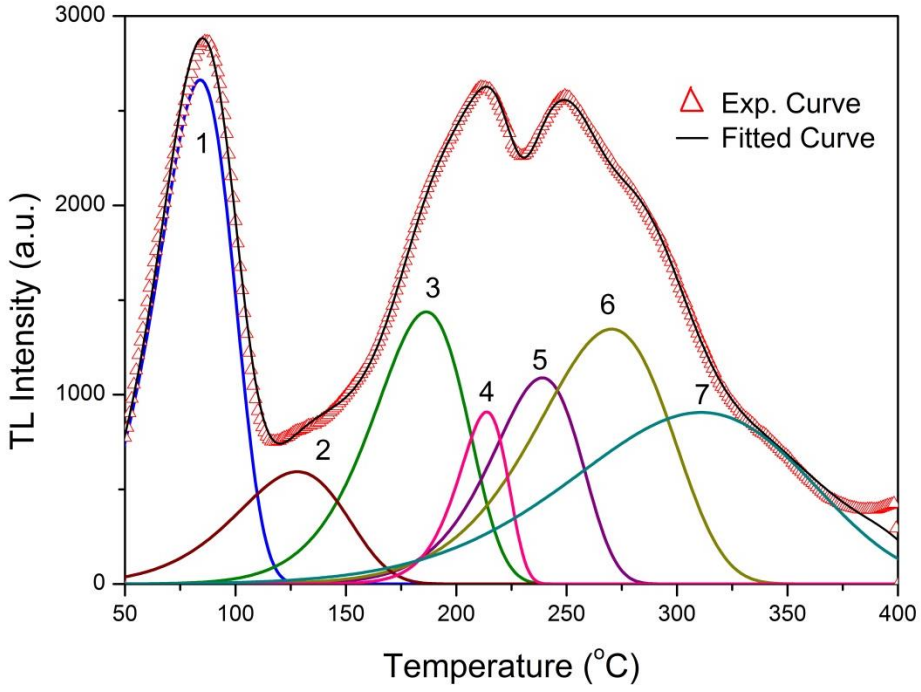

Figure 8. TL glow curve of the aventurine fitted with seven multiparameter functions.

The parameters (Tm, T1, T2, τ, δ, ω, μ, γ) which are calculated for each peak under deconvoluted experimental glow curve of aventurine are seen in Table 4. The symmetry factor (μg) determines the kinetic order of the thermoluminescence glow curve. The kinetic order is determined depending on the radiation peak shape. If the calculated μg value is found as 0.42, this is defined as first-order kinetic, and if it is 0.52, it is defined as second-order kinetic. [11]. The γ value defined as γ=δ/τ is another important factor in determining the kinetic orders. The range of γ=0.7–0.8 is for first-order kinetics, and the range of γ=1.05-1.20 is the value for second-order kinetics [14]. The parameter called the

merit number (FOM) determines the accuracy and suitability of the deconvolution process. The classification for FOM of deconvolution determined by this values; 0.0% - 2.5% the fit is good, 2.5% - 3.5% is small flow and > 3.5% is bad fit. [15,16].

Table 4. Kinetic parameters of aventurine for each deconvolution peak (FOM: 1.06).

Peak No	T_m(°C)	T_1	T_2	τ	δ	ω	μ_g	γ	E_{avg}(eV)	s (s^{-1})
1	84±1.2	61	102	23	18	41	0.439	0.782	0.663±0.013	$2.76x10^8$
2	127±3.1	94	154	33	27	60	0.450	0.818	0.580±0.024	$1.70x10^6$
3	186±2.4	157	208	29	22	51	0.431	0.758	0.857±0.014	$2,42x10^8$
4	214±1.5	198	225	16	11	27	0.407	0.687	1,707±0,046	$7,73x10^{16}$
5	239±2.6	211	260	28	21	49	0.428	0.750	1,109±0,009	$8,10x10^9$
6	270±3.2	229	301	41	31	72	0.430	0.756	0.833±0.024	$3.53x10^6$
7	310±3.6	240	368	70	58	128	0.453	0.828	0.556±0.046	$2.43x10^3$

3.5. Radioluminescence Properties

Radioluminescence (RL) is the luminescence that occurs when a material is excited by photon sources such as X-rays or gamma rays. In the radioluminescence process, X-ray or gamma beam excitation provides information about the whole sample, because penetrates the entire volume of the sample. With the radioluminescence spectrum, the emission intensity as a function of the wavelength of the excitation light, the excitation intensity as a function of the emitted wavelength, the polarization of the emission, and the quantum yield are examined. Ionizing radiation simultaneously activates existing optical centers, which enables the investigation of a material's luminescence properties. [17,18]. RL or X-ray excited luminescence is useful for determining defects of minerals. X-ray radiation penetrates and induces the whole volume of the sample, forming new luminescence defects. The radioluminescence emissions of minerals (for this research aventurine) or other luminescent materials (phosphors, ceramics, glass, fibers, etc.) were measured on a high-sensitivity wavelength-multiplexed CCD detector which is capable of detection range from 200 to1200 nm. So, in particular, the emission spectra of minerals with different impurity atoms can be determined in detail [19].

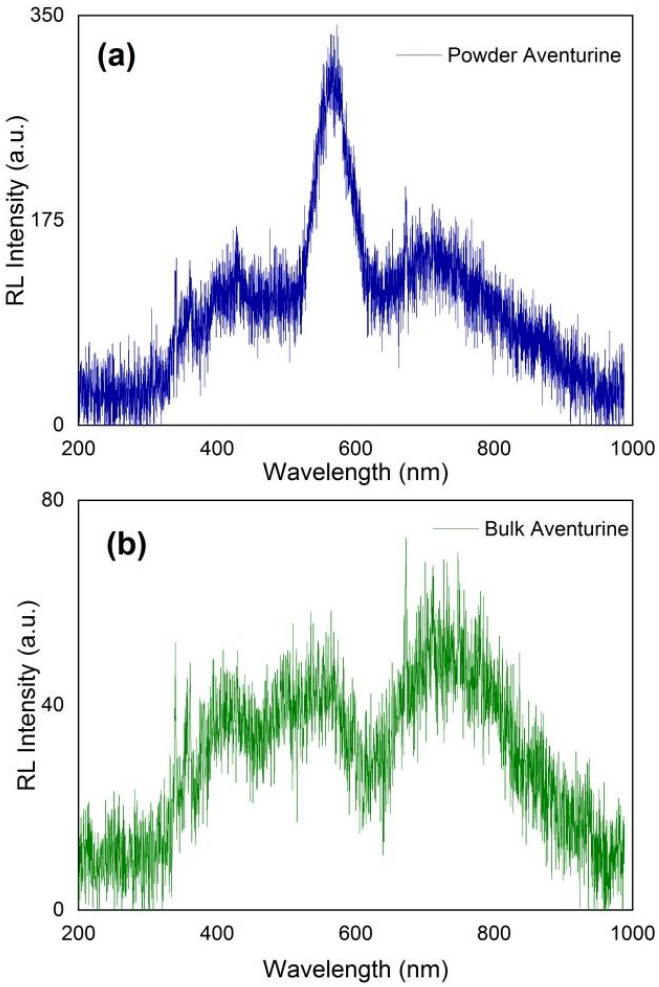

Figure 9. RL spectra of powder and bulk aventurine samples.

Fig. 9 shows the RL spectra of bulk and powder samples of aventurine. Aventurine has a quite broad emission range from about 300 to 1000 nm. Figure 9 (a) shows the emission bands of powder Aventurine with maximum peak intensities at approximately 360, 430, 570, 720, 870, and 890 nm. In Figure 9 (b), bulk aventurine exhibited emissions in almost the same regions, although the amount of noise was high due to the weakness of the detected luminescence.

It is seen that the emission intensity of the powder sample is five times higher than that of the bulk. In addition, although it is common to both the emission band with a peak maximum at 570 nm (quite weak in the bulk sample) became dominantly evident. In powder material, due to the easier penetration of X-rays compared to the bulk material, the reduction of the particle size, and the enlargement of the surface area, the luminescence collected by the detector as a result of volumetric interaction has a higher intensity.

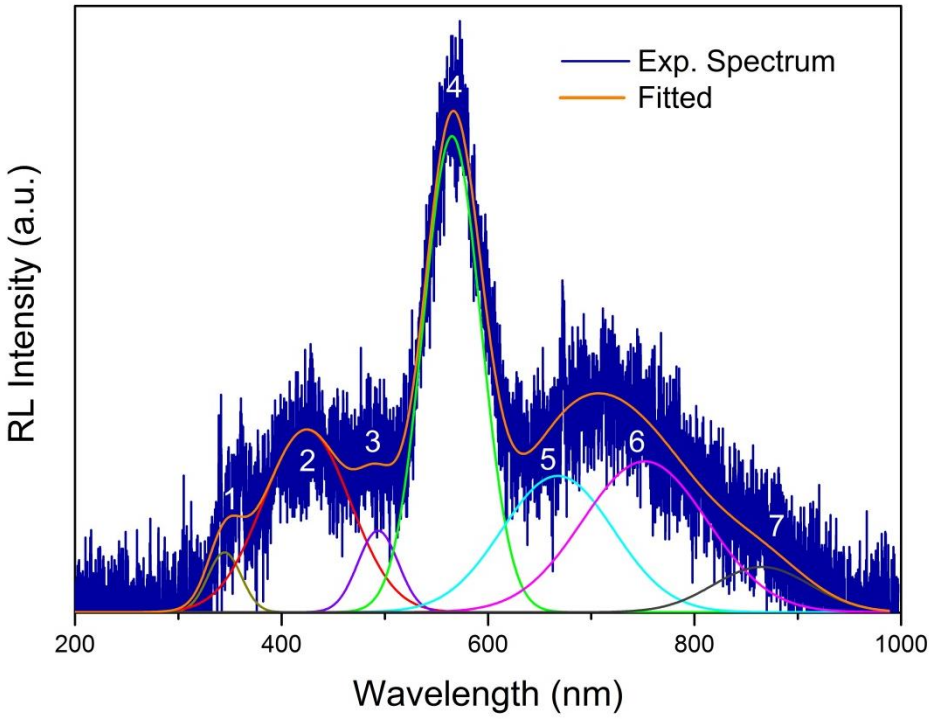

Figure 9. Fitted RL spectrum of powder aventurine.

In Fig. 10, suitable for the RL measurements is possible to determine, despite the complex structure of the RL emission behavior, that there are only a limited number of specific bands. The experimental RL spectrum, in the range of 200–1000 nm, was fitted by a sum of seven Gaussian functions using the fitting program. The factors involved in the luminescence phenomenon, which are emission spectra, lifetime, and efficiency, are the important parameters covered by luminescence. These parameters are directly dependent on the crystal phase, which is affected by factors such as temperature and pressure. Thus, minor changes in the lattice structure, such as impurities, the presence of surface defects or substitute ions, and inclusions at ppm concentrations, can cause changes in the intensity and wavelength position of the emission spectra [18].

Table 5. Parameters of possible peaks under the RL spectrum of aventurine.

Peak No	λ_{max} (nm)	I_{max} (a.u.)	A (peak area)	FWHM
1	344.83 ± 1.38	59.07± 2.11	1286.12 ± 153.30	37.96± 4.21
2	424.28 ± 1.81	124.42± 1.08	10287.39 ± 258.33	99.43 ± 7.79
3	493.46 ± 1.69	70.62± 1.27	2125.80 ± 132.38	46.02 ± 5.41
4	565.11 ± 0.60	280.68± 0.42	17840.35 ± 1093.79	66.12 ± 2.12
5	667.51 ± 2.66	99.78± 0.94	9822.08± 611.44	127.20 ± 1.38
6	751.93 ± 3.65	107.49± 1.12	12161.63± 1418.47	142.35 ± 7.69
7	865.14 ± 85.48	51.34± 2.07	2823.17 ± 563.18	110.04 ± 7.80

* Adj. R-Square 0.96513, λmax: the position of the maxima, Imax: intensity of the maxima, FWHM: full-width at half maximum

In Table 5 the parameters of the resolved possible peaks under the RL spectrum were given. Of course, it is possible to obtain many different variations apart from this deconvolution. Considering that each of the 7 individual peaks

corresponds to the emissions of impurity atoms contained in aventurine. We cannot say with certainty that the observed emission originates from a certain metal ion with a certain valence, but we should compare how well these overlap with examples in the literature. In Table 6, the emission wavelength values of Si, Mg, Fe, Al, and Ca ions, which were determined by the EDX analysis to be present in aventurine, are given in order from the highest intensity to the lowest. When Table 6 is examined, it is seen that there are emission values that are exactly compatible with the resolved peaks.

Table 6. The most intense spectral lines arranged according to wavelength [20].

Cations	Si^{1+}	Si^{2+}	Si^{3+}	Mg^{1+}	Mg^{2+}	Fe^{1+}	Fe^{2+}	Fe^{3+}	Al^{1+}	Al^{2+}	Al^{3+}
Wavelength (nm)	742	637	**455**	**880**	789	**868**	645	**437**	396	466	**360**
	728	**566**	386	518	448	649	624	592	**877**	600	414
	703	505	**573**	**552**	**439**	751	**730**	416	783	**559**	452
	594	**413**	482	382	-	**718**	542	428	669	835	**569**
	625	**333**	**348**	-	-	667	-	**360**	-	342	-
	855	784	761	-	-	-	-	-	-	-	-

Under stress structures with Si-O bonding, such as aventurine, have some unbounded oxygen or silicon-vacancy centers or some Si-O bonding defects, which cause UV emission. As for Cr, one of the important metals in Aventurine; Cr^{2+} ions exhibit a line emission at about 650 nm at room temperature. It is thought that this impurity emission may result from the $^3E \rightarrow {}^5E$ transition of the Cr^{2+} ion [21]. Although the measurement was taken at room temperature, it is known that the weak infrared emission at about 820 nm at low temperatures is related to the $^3E \rightarrow {}^3T_1$ transition of the Cr^{3+} ion [22].

A trivalent chromium ion (Cr^{3+}) is a significant transition metal member of the group. Chromium's $3d^3$ electron configuration has a really engaging combination of the spin doublet and spin-quartet states. Cr^{3+} has exhibited a wide emission from 650 nm to 850 nm in synthesized alumina-based phosphor. The stated wide emission band originated from the $^4T_{2g}$-$^4A_{2g}$ transition of Cr^{3+} [23]. It has been observed that the fluorescence spectra of glass-based optical fiber structures containing Cr^{3+} have a maximum peak around 540 nm in the range of 500-800 nm in the emission spectrum obtained as a result of 474 nm excitation [24].

4. Conclusions

Aventurine is a translucent form of quartz known for its bright containments which give it a sheeny look. The aventurine comes from the presence of chrome-bearing fuchsite, which adds a silvery green or silvery blue sheen to the crystal. Hematite or goethite subsumptions form orange and brown crystals. Aventurine can thus be found in various colors such as orange, blue, gray, brown, and yellow, but it is most often green. Minor phases of Fe and Cr were observed in the XRD analysis of Aventurine, a silicon oxide-based mineral. In the EDX spectrum, the presence of Mg, Al, Cr, and Fe was detected, except for Si and O. TL glow curves of the sample irradiated with UV light and X-ray radiation for 10, 20, and 30 minutes were examined. As a result of UV irradiation, it was observed that deep traps at high temperatures were more prominent and had a main peak with a maximum intensity of about 300 oC. It has been determined that both shallow traps and deep traps are strongly present in the glow curves obtained after X-ray irradiation. CGDC analysis

was performed on the curve obtained after 900 Gy dosing, and it was observed that the resolved peaks were first-order kinetic levels, varying from 0.663±0.013 eV to 1.707±0.046 eV. The RL spectra of powder and bulk Aventurine samples generally showed similar emissions, but the powder sample has a strong emission of around 560 nm. In order to determine the possible positions of the Gaussian peaks which are forming this main emission spectrum consists of and the caused by the impurity atoms, the RL spectrum was also deconvolved. Depending on the presence of ions in aventurine, the formation mechanism of emissions is discussed.

References

[1] B. Karasu, B. Sarıcaoğlu, Aventurin Sırlarına Genel Bir Bakış, El-Cezeri Fen ve Mühendislik Derg. 2019 (2019) 140–155. doi:10.31202/ecjse.460093.

[2] M.J.O. Donoghue, eJournal of Gemmology Gemmologıcal Assocıatıon Of Great Brıtaın, 20 (1986).

[3] A. Gozalbo, M.J. Orts, S. Mestre, P. Agut, F. Lucas, A. Belda, C. Blanco, Ceramic Glazes With Aventurine Effect, Cycle. (2006) 189–202.

[4] M.D. Shcheglova, M e c h a n i s m of a v e n t u r i n e f o r m a t i o n 1~ c o p p e r - c o n t a i n i n g a l k a l i - l e a d silicate glass, Glas. Ceram. 53 (1996) 14–17.

[5] M.I. Kati, M. Türemis, I.C. Keskin, B. Tastekin, R. Kibar, A. Çetin, N. Can, Luminescence behaviour of beryl (aquamarine variety) from Turkey, J. Lumin. 132 (2012). doi:10.1016/j.jlumin.2012.03.058.

[6] İ.Ç. Keskin, M.İ. Katı, M. Türemiş, A. Çetin, Y. Tuncer Arslanlar, R. Kibar, Determination of Thermoluminescence Kinetic Parameters of White and Blue Chalcedony Exposed to X-ray Irradiation, Radiat. Phys. Chem. (2018). doi:10.1016/j.radphyschem.2018.05.031.

[7] M.I. Teixeira, D.N. Souza, L.V.E. Caldas, Onyx as radiation detector for high doses, Radiat. Meas. 46 (2011) 1894–1896. doi:10.1016/j.radmeas.2011.07.021.

[8] S. Gültekin, S. Yıldırım, O. Yılmaz, İ.Ç. Keskin, M.İ. Katı, E. Çelik, Structural and optical properties of SrAl2O4: Eu2+/Dy3+ phosphors synthesized by flame spray pyrolysis technique, J. Lumin. 206 (2019) 59–69. doi:10.1016/j.jlumin.2018.10.011.

[9] R. Ullah, B.K. Deb, M. Yousuf, A. Mollah, Synthesis and Characterization of Silica Coated Iron-Oxide Composites of Different Ratios, Int. J. Compos. Mater. 4 (2014) 135–145. doi:10.5923/j.cmaterials.20140402.13.

[10] V. Ramasamy, P. Rajkumar, V. Ponnusamy, Depth wise analysis of recently excavated Vellar river sediments through FTIR and XRD studies, Indian J. Phys. 83 (2009) 1295–1308. doi:10.1007/s12648-009-0110-3.

[11] C. Pagonis, Vasilis, Kitis, George, Furetta, Numerical and Practical Exercises in Thermoluminescence, Springer New York, New York, NY, 2006. doi:10.1007/0-387-30090-2.

[12] T. Sakurai, R.K. Gartia, Method of computerized glow curve deconvolution for analysing thermoluminescence, J. Phys. D. Appl. Phys. 36 (2003) 2719–2724. doi:10.1088/0022-3727/36/21/020.

[13] N.D. Sang, N. Van Hung, T. Van Hung, N.Q. Hien, Using the computerized glow curve deconvolution method and the R package tgcd to determination of thermoluminescence kinetic parameters of chilli powder samples by GOK model and OTOR one, Nucl. Instruments Methods Phys. Res. Sect. B Beam Interact. with Mater. Atoms. 394 (2017) 113–120. doi:10.1016/j.nimb.2017.01.012.

[14] M. Balarin, Half-width and asymmetry of glow peaks and their consistent analytical representation, J. Therm. Anal. 17 (1979) 319–332. doi:10.1007/BF01914023.

[15] H.G. Balian, N.W. Eddy, Figure-of-merit (FOM), an improved criterion over the normalized chi-squared test for assessing goodness-of-fit of gamma-ray spectral peaks, Nucl. Instruments Methods. 145 (1977) 389–395. doi:10.1016/0029-554X(77)90437-2.

[16] S.K. Misra, N.W. Eddy, IFOM, a formula for universal assessment of goodness-of-fit of gamma ray spectra, Nucl. Instruments Methods. 166 (1979) 537–540. doi:10.1016/0029-554X(79)90546-9.

[17] A.T.Y. Arslanlar Tuncer Y., Kibar R., Çetin A., Canımoğlu A., Radioluminescence Properties of Copper- and Terbium-Implanted Strontium Titanate Radioluminescence Properties of Copper- and Terbium-Implanted Strontium Titanate, Lett. Spectrosc. (2013) 364–366. doi:10.1080/00387010.2012.738278.

[18] Y. Rodríguez-Lazcano, V. Correcher, J. Garcia-Guinea, Thermo- and cathodoluminescence properties of lepidolite, Spectrochim. Acta - Part A Mol. Biomol. Spectrosc. 113 (2013) 281–285. doi:10.1016/j.saa.2013.04.107.

[19] Y. Tuncer Arslanlar, J. Garcia-Guinea, R. Kibar, A. Çetin, M. Ayvacikli, N. Can, Luminescence behavior and Raman characterization of jade from Turkey, Appl. Radiat. Isot. 69 (2011) 1299–1306. doi:10.1016/j.apradiso.2011.05.011.

[20] A.R. Striganov, N.S. Sventitskii, Tables of Spectral Lines of Neutral and Ionized Atoms, Springer US, Boston, MA, 1968. doi:10.1007/978-1-4757-6610-3.

[21] Y.T. Arslanlar, Doğal Taşların Ve Sentetiklerinin Karakteristik Ve Optik Özelliklerinin İncelenmesi Doktora Tezi Yasemin Tuncer Arslanlar, Celal Bayar Üniversitesi Fen Bilimleri Enstitüsü, 2011.

[22] T.C. Vanoy, A.M. Levert, G.L. McPherson, Luminescence spectra of crystals of RbMnCl 3 , Rb 2 MnCl 4 and CsMnBr 3 doped with Cr 2+ : exciton trapping at luminescent Cr 2+ centres, J. Phys. C Solid State Phys. 21 (1988) 2969–2979. doi:10.1088/0022-3719/21/15/027.

[23] L. Zhang, S. Zhang, Z. Hao, X. Zhang, G. Pan, Y. Luo, H. Wu, J. Zhang, A high efficiency broad-band near-infrared Ca 2 LuZr 2 Al 3 O 12 :Cr 3+ garnet phosphor for blue LED chips, J. Mater. Chem. C. 6 (2018) 4967–4976. doi:10.1039/C8TC01216D.

[24] D. Dutta, A. Dhar, A. V. Kir'yanov, S. Das, S. Bysakh, M.C. Paul, Fabrication and characterization of chromium-doped nanophase separated yttria-alumina-silica glass-based optical fibers, Phys. Status Solidi. 212 (2015) 1836–1844. doi:10.1002/pssa.201532017.